Supplementary Material

SI. Pseudo Code of AMNC

Algorithm 1 Adaptive Modular Neural Control (AMNC)

Input: positional feedback
Output: positional command
# update adaptation signals
for $x \in joint\ modules$ **do**
  update GA^x according to Section III-B1
  update CA^x according to Section III-B2
end for
# update main network
for $x \in joint\ modules$ **do**
  update CPG^x according to Section III-A1
  update RBF^x according to Section III-A2
  update FD^x according to Section III-A3
end for
# control the exoskeleton
return/send positional command to the exoskeleton

SII. Preliminary Experiment: Parameter Analysis

To verify that applying the forcing term at the position level of the FD (according to Section III-A3) is more accurate than applying it at the velocity level [S14] (according to Eqs. S1–S3), a preliminary parameter analysis was performed in simulation.

$$\ddot{\theta}[t] = \alpha\left(\beta(\bar{\theta}[t-1] - \theta[t-1]) - \dot{\theta}[t-1]\right) + k_a\dot{I}[t], \quad \text{(S1)}$$

$$\dot{\theta}[t] = \dot{\theta}[t-1] + \tau\ddot{\theta}[t] + f[t] + k_v I[t], \quad \text{(S2)}$$

$$\theta[t] = \theta[t-1] + \tau\dot{\theta}[t], \quad \text{(S3)}$$

where θ[t], $\dot{\theta}[t]$, $\ddot{\theta}[t]$ denote the output of θ, $\dot{\theta}$, and $\ddot{\theta}$ at timestep t, respectively; $\theta[t]$ represents the position profile passing to the low-level position control at timestep t; $f[t]$ denotes the forcing term at timestep t; $\bar{\theta}[t]$ denotes the target joint trajectory at timestep t; τ represents the time constant; $I[t]$ and $\dot{I}[t]$ denote the impedance-based adaptation signals from the CA at timestep t; k_v, k_a, α, and β denote the gains.

The objective was to compare the imitation accuracy at the 20th gait cycle. Accordingly, the adaptation signals from both the CA and the GA were set to zero (i.e., setting k_v and k_a to zero). Four non-adaptable controls were then tested: (1) the control with the forcing term applied at the velocity level where α and β were set to 0.4 and 0.1, respectively; (2) the control with the forcing term applied at the velocity level where α and β were set to 4.0 and 1.0, respectively; (3) the control with the forcing term applied at the position level where α and β were set to 0.4 and 0.1, respectively; and (4) the control with the forcing term applied at the position level where α and β were set to 4.0 and 1.0, respectively. The root-mean-square error was calculated and compared to the target (i.e., default positional trajectory of Exo-H3 [S15]). Finally, the results are presented in Fig. S1.

The results presented in Fig. S1 indicate that the position form (i.e., applying the forcing term on position level of the FD) yields a lower fitting error than the velocity form (i.e., applying the forcing term at the velocity level of the FD). This is because the velocity form integrates the fitting error at every timestep, thereby resulting in a poor fitting performance [S19]. Moreover, although α and β are crucial in improving fitting accuracy in velocity form, they exert a minimal effect on the position form. Therefore, this study utilizes the FD with the position form as discussed in Section III-A3.

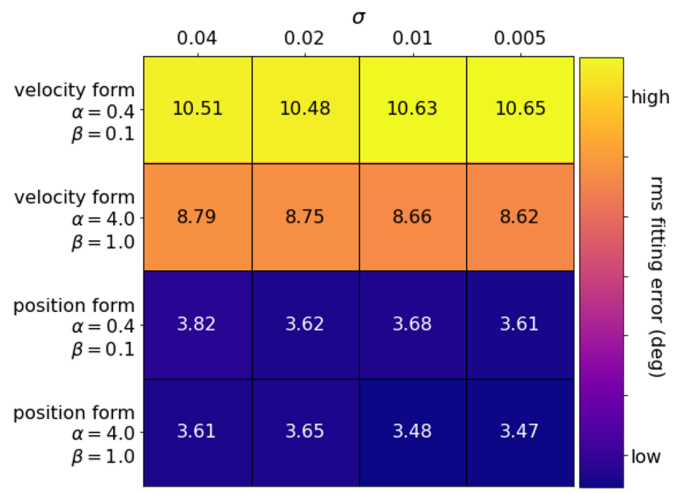

Fig. S1: Root-mean-square fitting error comparison between the forward dynamics network in the position form and that in the velocity form with different sets of parameters at the 20th cycle.

SIII. Time Series Plot

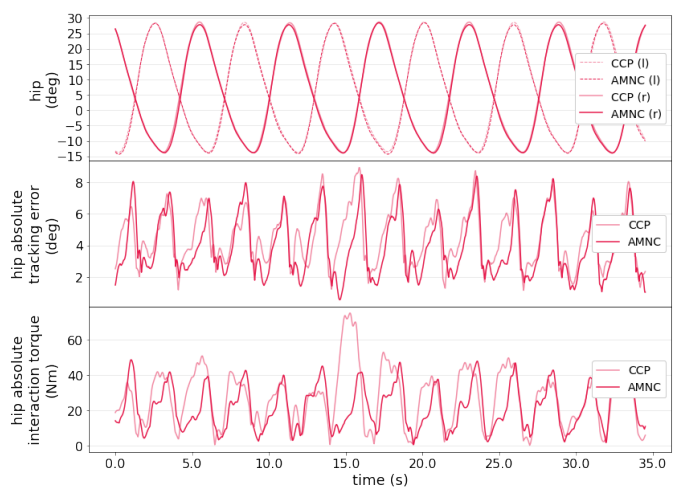

Fig. S2: Positional command, absolute tracking error, and absolute interaction torque of the hip joints.

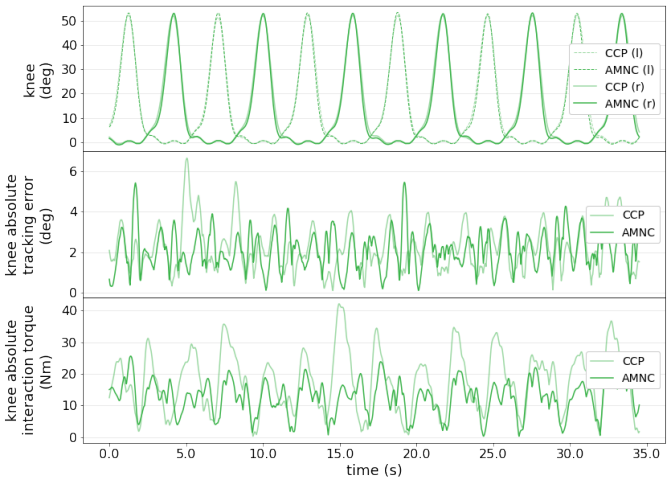

Fig. S3: Positional command, absolute tracking error, and absolute interaction torque of the knee joints.

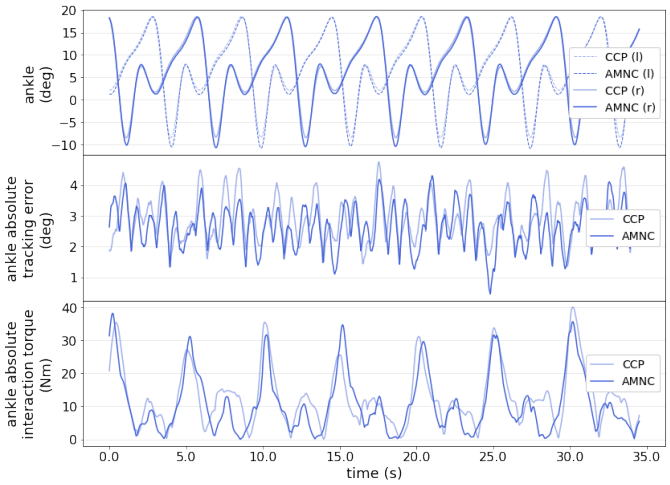

Fig. S4: Positional command, absolute tracking error, and absolute interaction torque of the ankle joints.

SIV. Walking on Different Slopes

We verified our key hypothesis that the proposed AMNC can improve the assistance performance of the exoskeleton in walking on a level floor. To further demonstrate the effectiveness of the proposed AMNC in different unknown conditions, we conducted an additional experiment where we tested it on different slopes and compared it with the benchmark CCP. In this experiment, the BERTEC treadmill was employed to simulate walking on different slopes (i.e., a treadmill with varying slope angles). The subject started walking on a 0° slope (a level floor). During walking, the treadmill was progressively inclined to certain angles (4° and 8°), simulating walking up slopes, and then gradually declined to 0°. Note that the control parameters of both controllers, which were initially designed for level floor walking, were applied to this experiment. This is to assess the capabilities of both controllers in terms of the generalization and adaptability to unexpected changing conditions.

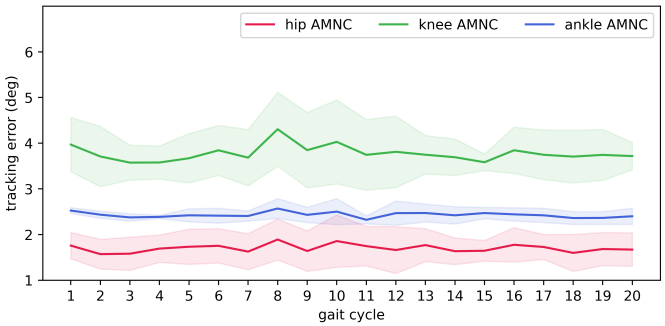

Fig. S5: Hip, knee, and ankle root-mean-square tracking errors obtained from the AMNC-based control. The results are averaged over the test subjects, corresponding to Fig. 7. There are no significant changes in the absolute tracking errors ($\leq 1^o$) of all joints across gait cycles. For example, tracking errors between the first and last gait cycles are 0.08 ± 0.29^o (hip), 0.25 ± 0.45^o (knee), and 0.12 ± 0.20^o (ankle), and those between the second last and last gait cycles are 0.01 ± 0.25^o (hip), 0.02 ± 0.35^o (knee), and -0.03 ± 0.10^o (ankle). This implies that the proposed AMNC can immediately adapt the exoskeleton and maintain its maximum acceptable performance (i.e., all tracking errors $\leq 5^o$) within the first gait cycle (or "≈ 0 gait cycle" convergence). This acceptable error range is defined from the fact that the exoskeleton still allows for walking with clear swing, stand, and double support phases. Note that the differences in the hip, knee, and ankle joint tracking errors are expected to be a result of human interaction. For example, the hip tracking error might be the lowest because the hip joint is easier to synchronize compared with the other joints. Further analysis may go beyond the scope of this work and therefore needs to be investigated in future studies.

The results obtained from the experiment are presented in Fig. S7. The varying slope angle, average tracking errors of all joints from both controllers, average interaction torques of all joints from both controllers, and their moving average values are provided. The video of the experiment is also available at https://youtu.be/BUSyHQ0Grf0 (the proposed AMNC).

It can be observed that the tracking error of the CCP control was overshoot at the beginning of all transitions (refer to Fig. S7 at approximately 25 s, 100 s, and 175 s). This is because the subject had to alter his gait to cope with new conditions and the CCP control was unable to quickly adapt to the new conditions properly. In contrast, the AMNC could effectively handle the new conditions resulting in low tracking error. Comparing the interaction torque of both controllers, the AMNC exhibited lower interaction torque than the CCP throughout the entire experiment. In addition, it can be observed that the peaks of the interaction torque from the CCP control are greater than those from the AMNC in almost all gait cycles. This suggests that the proposed AMNC is not limited to level floor walking, as it can also assist a user on different terrains/environments by improving motion synchronization (i.e., tracking error) and reducing the interaction torque.

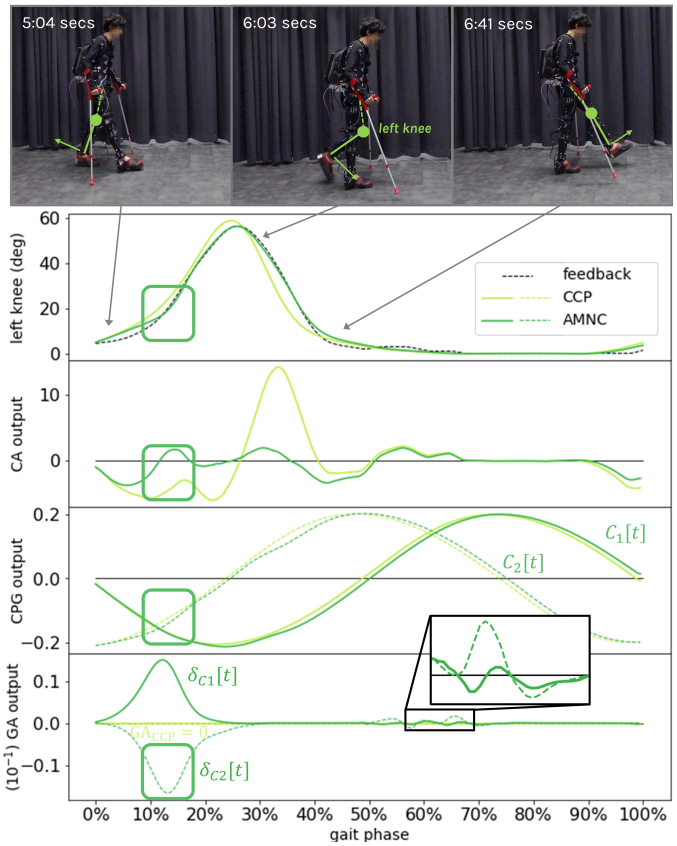

Fig. S6: The control Control command, feedback trajectories, CPG outputs, and adaptation signals from the CA and GA of the left knee module. The signals were evaluated with the AMNC and CCP control. Note that the GA signals of the benchmark CCP control remain continuously at zero since as they do not have the gradient-based adaptation mechanism.

SV. Method Comparison

In Table SI, CPG refers to a central pattern generator or a mechanism related to a periodic pattern generator/oscillator; RBF refers to a radial basis function network or a mechanism related to pattern shaping/adaptation; FD refers to a forward dynamics network or a mechanism related to system dynamics simulation; CA refers to a couple cooperative primitive-based adaptation network or a mechanism related to online impedance-based adaptation feedback; GA refers to the gradient-based adaptation network or a mechanism related to online gradient-based adaptation feedback.

SVI. Code and Video

The program and simulation adopted in this study are available at https://github.com/Arthicha/EXOVIS_AMNC, while the videos of the experiments are available at https://www.youtube.com/watch?v=AMjdBNzH4Lg (walking on a level floor), and https://youtu.be/BUSyHQ0Grf0 (walking on different slopes).

TABLE SI: Comparison between the state-of-the-art methods and the proposed AMNC in terms of equivalent modules: CPG, RBF, FD, CA, and GA. Note that ✓and ✗ denote inclusion and exclusion, respectively.

Methods	CPG	RBF	FD	CA	GA
LINECOSPAR [S5]	✗	✗	✗	✗	✗
AFO [S6]	✓	✓	✗	✗	✗
FHAE [S7]	✓	✓	✗	✗	✗
PSAO [S8]	✓	✓	✗	✗	✗
GEMS [S9]	✓	✓	✗	✗	✗
DMP-HIL [S10]	✓	✓	✓	✗	✗
DDOC [S11]	✓	✓	✗	✗	✗
CCP-HIL [S14]	✓	✓	✓	✓	✗
CCP [S14]	✓	✓	✓	✓	✗
SO(2) [S16]	✓	✗	✗	✗	✗
AMNC (OURS)	✓	✓	✓	✓	✓

SVII. Parameter Table

All the parameters/variables used in the AMNC along with their values and selection methods are summarized in Table SII.

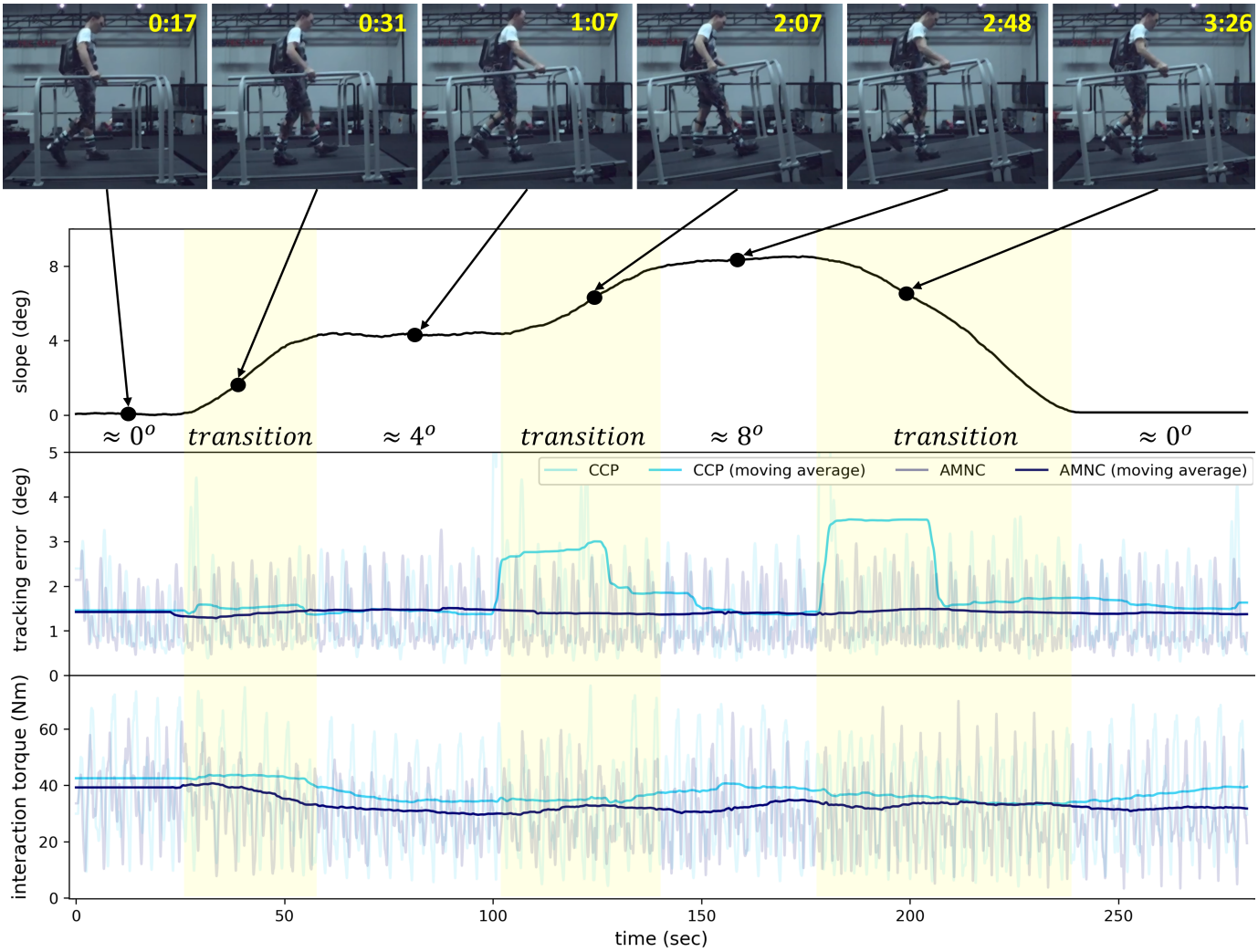

Fig. S7: Varying slope angle, average tracking errors of all joints, average interaction torques of all joints, and their moving average values. The signals obtained from the benchmark CCP control (light blue) and the proposed AMNC control (dark blue) are compared over time.

TABLE SII: Parameters/variables in the AMNC along with their definitions, values, and selection methods.

Parameter	Meaning	Value	Selection
$C_j[t]$	output of neuron C_j (i.e., output j of the CPG) at timestep t	vary	Eqs. 2 and 3
$\delta^x_{C_j}[t]$	CPG adaptation signal from GA of joint x passing to C_j at timestep t	vary	Eq. 11
w_{11}	weight of the recurrent connection of C_1	1.0087	according to [S16]
w_{12}	weight of the connection from C_2 to C_1	0.0497	according to [S16]
w_{22}	weight of the recurrent connection of C_2	1.0087	according to [S16]
w_{21}	weight of the connection from C_1 to C_2	-0.0497	according to [S16]
$K_i[t]$	the output of K_i (i.e., an RBF kernel) at timestep t	vary	Eq. 4
$R_{ji}[t]$	the center of the RBF function corresponding to C_j and K_i	fixed	i^{th} interpolation of non-adapted C_j
σ	scaling gain	0.01	empirically selected to obtained smooth signal
$f[t]$	output of f (i.e., the forcing term) at timestep t	vary	Eq. 5
w_{fi}	weight of the connection from neuron K_i to f	fixed	Eq. 6
w_{ji}	weight of the connection from neuron i^{th} to j^{th}	fixed	depends on the function
$\ddot{\theta}[t]$	output of $\ddot{\theta}$, representing acceleration at timestep t	vary	Eq. 7
$\dot{\theta}[t]$	output of $\dot{\theta}$, representing velocity at timestep t	vary	Eq. 8
$\theta[t]$	output of θ, representing positional command at timestep t	vary	Eq. 9
$\theta^*[t]$	output of θ^*, representing positional feedback at timestep t	vary	sensory feedback
$\bar{\theta}[t]$	target joint trajectories at timestep t	fixed	Exo-H3 [S15]
α	gain of the FD	1.0	according to [S14]
β	gain of the FD	4.0	according to [S14]
k_v	gain of the FD	2.5	empirically selected to obtained fast response without oscillation
k_a	gain of the FD	1.8	empirically selected to obtained fast response without oscillation
ρ	learning rate for offline RBF training	0.01	empirically selected to obtain minimum error
τ	time constant	1	represent a timestep
T	sampling point of the target joint trajectory	128	depends on the target joint trajectory
$I[t]$	impedance-based adaptation signals from the CA at timestep t	vary	Eq. 16
$\dot{I}[t]$	impedance-based adaptation signals from the CA at timestep t	vary	Eq. 17
η	adaptation gain of the GA	0.2	empirically selected to obtained fast response without oscillation
$e[t]$	output of e (i.e., the tracking error) at timestep t	vary	Eq. 12
$\mu_{ji}[t]$	output of μ_{ji} at timestep t	vary	Eq. 13
$\psi_j[t]$	output of ψ_j at timestep t	vary	Eq. 14
k_p	gain of the CA	2.5	empirically selected to obtained fast response without oscillation
k_d	gain of the CA	1.8	empirically selected to obtained fast response without oscillation

References

[S1] Libo Zhou, Weihai Chen, Wenjie Chen, Shaoping Bai, Jianbin Zhang, and Jianhua Wang. Design of a passive lower limb exoskeleton for walking assistance with gravity compensation. *Mechanism and Machine Theory*, 150:103840, 2020.

[S2] Nicholas A Bianco, Patrick W Franks, Jennifer L Hicks, and Scott L Delp. Coupled exoskeleton assistance simplifies control and maintains metabolic benefits: a simulation study. *bioRxiv*, 2021.

[S3] Romain Baud, Ali Reza Manzoori, Auke Ijspeert, and Mohamed Bouri. Review of control strategies for lower-limb exoskeletons to assist gait. *Journal of NeuroEngineering and Rehabilitation*, 18(1):1–34, 2021.

[S4] Gian Maria Gasparri, Michael Owen Bair, Robert Patrick Libby, and Zachary Forest Lerner. Verification of a robotic ankle exoskeleton control scheme for gait assistance in individuals with cerebral palsy. In *2018 IEEE/RSJ International Conference on Intelligent Robots and Systems (IROS)*, pages 4673–4678. IEEE, 2018.

[S5] Maegan Tucker, Myra Cheng, Ellen Novoseller, Richard Cheng, Yisong Yue, Joel W Burdick, and Aaron D Ames. Human preference-based learning for high-dimensional optimization of exoskeleton walking gaits. In *2020 IEEE/RSJ International Conference on Intelligent Robots and Systems (IROS)*, pages 3423–3430. IEEE, 2020.

[S6] Hamidreza Talatian, Mohammad Karami, Hamed Moradi, and Gholamreza Vossoughi. Design and implementation of an intelligent control system for a lower-limb exoskeleton to reduce human energy consumption. In *2021 10th International Conference on Modern Circuits and Systems Technologies (MOCAST)*, pages 1–4. IEEE, 2021.

[S7] Tao Xue, Ziwei Wang, Tao Zhang, and Meng Zhang. Adaptive oscillator-based robust control for flexible hip assistive exoskeleton. *IEEE Robotics and Automation Letters*, 4(4):3318–3323, 2019.

[S8] Keehong Seo, SeungYong Hyung, Byung Kwon Choi, Younbaek Lee, and Youngbo Shim. A new adaptive frequency oscillator for gait assistance. In *2015 IEEE International Conference on Robotics and Automation (ICRA)*, pages 5565–5571. IEEE, 2015.

[S9] Keehong Seo, Kyungrock Kim, Young Jin Park, Joon-Kee Cho, Jongwon Lee, Byungjune Choi, Bokman Lim, Younbaek Lee, and Youngbo Shim. Adaptive oscillator-based control for active lower-limb exoskeleton and its metabolic impact. In *2018 IEEE International Conference on Robotics and Automation (ICRA)*, pages 6752–6758. IEEE, 2018.

[S10] Rui Huang, Hong Cheng, Hongliang Guo, Xichuan Lin, and Jianwei Zhang. Hierarchical learning control with physical human-exoskeleton interaction. *Information Sciences*, 432:584–595, 2018.

[S11] Zhinan Peng, Rui Luo, Rui Huang, Tengbo Yu, Jiangping Hu, Kecheng Shi, and Hong Cheng. Data-driven optimal assistance control of a lower limb exoskeleton for hemiplegic patients. *Frontiers in Neurorobotics*, 14:37, 2020.

[S12] Shiyin Qiu, Wei Guo, Darwin Caldwell, and Fei Chen. Exoskeleton online learning and estimation of human walking intention based on dynamical movement primitives. *IEEE Transactions on Cognitive and Developmental Systems*, 13(1):67–79, 2020.

[S13] Andres Martinez, Brian Lawson, Christina Durrough, and Michael Goldfarb. A velocity-field-based controller for assisting leg movement during walking with a bilateral hip and knee lower limb exoskeleton. *IEEE Transactions on Robotics*, 35(2):307–316, 2018.

[S14] Rui Huang, Hong Cheng, Jing Qiu, and Jianwei Zhang. Learning physical human–robot interaction with coupled cooperative primitives for a lower exoskeleton. *IEEE Transactions on Automation Science and Engineering*, 16(4):1566–1574, 2019.

[S15] Robotic Exoskeleton Exo-H3 Technaid—Leading Motion. https://www.technaid.com/, 2021. accessed: 2021-08-07.

[S16] Frank Pasemann, Manfred Hild, and Keyan Zahedi. SO(2)-networks as neural oscillators. In *International Work-Conference on Artificial Neural Networks*, pages 144–151. Springer, 2003.

[S17] Mathias Thor, Tomas Kulvicius, and Poramate Manoonpong. Generic neural locomotion control framework for legged robots. *IEEE transactions on neural networks and learning systems*, 32(9): 4013–4025, 2020.

[S18] Sebastian Ruder. An overview of gradient descent optimization algorithms. *arXiv preprint arXiv:1609.04747*, 2016.

[S19] Emre Sariyildiz and Hakan Temeltas. Performance analysis of numerical integration methods in the trajectory tracking application of redundant robot manipulators. *International Journal of Advanced Robotic Systems*, 8(5):63, 2011.

[S20] E. Rohmer, S. P. N. Singh, and M. Freese. V-rep: A versatile and scalable robot simulation framework. In *2013 IEEE/RSJ International Conference on Intelligent Robots and Systems*, pages 1321–1326, 2013. doi: 10.1109/IROS.2013.6696520.

[S21] Auke Jan Ijspeert, Jun Nakanishi, and Stefan Schaal. Movement imitation with nonlinear dynamical systems in humanoid robots. In *Proceedings 2002 IEEE International Conference on Robotics and Automation (Cat. No. 02CH37292)*, volume 2, pages 1398–1403. IEEE, 2002.

[S22] Zhenlei Chen, Qing Guo, Tieshan Li, Yao Yan, and Dan Jiang. Gait prediction and variable admittance control for lower limb exoskeleton with measurement delay and extended-state-observer. *IEEE Transactions on Neural Networks and Learning Systems*, 2022.

[S23] Yi Long, Zhi-jiang Du, Wei-dong Wang, and Wei Dong. Human motion intent learning based motion assistance control for a wearable exoskeleton. *Robotics*

and Computer-Integrated Manufacturing, 49:317–327, 2018.

[S24] Lincong Luo, Liang Peng, Chen Wang, and Zeng-Guang Hou. A greedy assist-as-needed controller for upper limb rehabilitation. *IEEE transactions on neural networks and learning systems*, 30(11):3433–3443, 2019.

[S25] Jettanan Homchanthanakul and Poramate Manoonpong. Continuous online adaptation of bioinspired adaptive neuroendocrine control for autonomous walking robots. *IEEE Transactions on Neural Networks and Learning Systems*, 33(5):1833–1845, 2021.

[S26] Adriana Torres-Pardo, David Pinto-Fernández, Manolo Garabini, Franco Angelini, David Rodriguez-Cianca, Stefano Massardi, Jesús Tornero-López, Juan C Moreno, and Diego Torricelli. Legged locomotion over irregular terrains: State of the art of human and robot performance. *Bioinspiration & Biomimetics*, 2022.